Original Article

STAT1-p53-p21axis-dependent stress-induced progression of chronic nephrosis in adriamycin-induced mouse model

Hua Wei, Jiali Wang, Zhaozhi Liang

Nephrology Department, Xinxiang Central Hospital, Xinxiang, China

Contributions: (I) Conception and design: H Wei; (II) Administrative support: J Wang; (III) Provision of study materials or patients: H Wei, Z Liang; (IV) Collection and assembly of data: All authors; (V) Data analysis and interpretation: H Wei, JWang; (VI) Manuscript writing: All authors; (VII) Final approval of manuscript: All authors.

Correspondence to: Hua Wei. Nephrology Department, Xinxiang Central Hospital, No. 56 Jinsui Avenue, Xinxiang, China. Email: 15637359221@163.com.

Background: Chronic nephrosis (CN) is an aging-related disease with high mortality. Signal transduction and transcriptional activator 1 (STAT1) protein promotes senescence in human glomerular mesangial cells (HMCs), but whether it affects the progression of adriamycin (ADR)-induced CN *in vivo* remains unclear.

Methods: We established an ADR-induced CN mouse model that was completed in wild-type (wt) mice by a single intravenous injection of 10 mg/kg ADR for 2 or 4 weeks. Clinical indexes in each group were determined. Hematoxylin and eosin staining (H&E) was employed to determine renal histopathological damage, SA-β-gal staining was used to evaluate cell senescence phenotype. TUNEL and immunohistochemistry (IHC) staining were used to detect renal apoptosis. Protein levels of Bcl-2, Bax, STAT1, p53 and p21 were measured by Western Blot.

Results: STAT1 intervention ameliorated renal function. H&E staining indicated that STAT1-deficient (*stat1*$^{-/-}$) improved the renal tubular injury, and *stat1*$^{-/-}$ obviously inhibited the apoptosis and Caspase-3^{+} number in kidney tissues. Besides, *stat1*$^{-/-}$ decreased proteinuria, and the levels of urea nitrogen and creatinine as well as that of reactive oxygen species induced by ADR. Also, *stat1*$^{-/-}$ resulted in the reduced expression of p53 and p21.

Conclusions: Our current study strongly demonstrated the involvement of the STAT1-p53-p21 axis in the regulation of CN and is a potential target for the nephrosis treatment.

Keywords: Adriamycin; chronic nephrosis (CN); mitogen-activated protein kinase; senescence; STAT1

Submitted Jun 19, 2020. Accepted for publication Jul 29, 2020. This article was updated on August 27, 2021.
The original version was available at: http://dx.doi.org/10.21037/atm-20-5167
doi: 10.21037/atm-20-5167

Introduction

Chronic nephrosis (CN) has a high mortality rate. It is the end result of renal structural change and dysfunction caused by multiple factors over a time course of more than 3 months, finally progressing to end stage renal disease (ESRD), namely uremia (1). With aging populations and the increasing prevalence of hypertension and diabetes, the number of cases of CN has been gradually increasing (2). Without timely and appropriate treatment, nephrosis patients who will develop end-stage renal diseases and seriously reduce their quality of life (3). Therefore, it is of great significance to understand the mechanism of CN. In the development of renal pathology, the application of hormone and immunosuppressive agents is a milestone in the diagnosis and treatment of renal disease (4). Unfortunately, there are no specific clinical drugs and/or treatments for CN treatment. So, it is urgent to explore new pathogenesis and treatment strategies of CN.

Signal transduction and transcriptional activator (STAT) is a transcription factor located in the cytoplasm. The STAT family mainly comprises STAT1, STAT2, STAT3, STAT4, STAT5 (a/b) and STAT6, which are activated when various extracellular stimuli, such as cytokines and growth

factors, bind to specific receptors on the cell surface (5). STATs are activated by phosphorylation of the conserved tyrosine and serine by Janus kinases and mitogen-activated protein kinases in the c-terminal transcriptional activation region (6). Activated STATs can translocate into nuclei in the form of heterogeneous or homologous dimers, then bind to targeted sequences in the promoter region, thus regulating biological processes such as cell proliferation, survival, apoptosis and differentiation (6).

The STAT1-p53-p21 axis has been elaborated in detail. First, STAT1 negatively regulates the p53 inhibitor *MDM2* (murine double minute 2) gene, thereby increasing the expression of p53, and the expression level of MDM2 is increased in STAT1-deficient cells (7). In addition, STAT1 can directly interact with p53, acting as a co-activator and regulating the functional activity of p53 responsive genes (8). Second, activated STAT1 can specifically bind to the conserved STAT1 response element in the p21 promoter region, and positively regulate the expression of p21 (9), leading to cell cycle arrest or apoptosis (9,10). Therefore, after activation of STAT1, p21 can be increased through dependent or independent p53 pathways. In summary, the downstream genes *p53* and *p21* regulated by STAT1 are senescence-related genes. Therefore, the STAT1-p53-p21 signal axis may be involved in senescence. Our initial *in vitro* experiments proved that the STAT1-p53-p21 signal axis can indeed regulate the senescence of human glomerular mesangial cells (HMCs) under stress conditions (11).

Adriamycin (ADR), an antitumor drug isolated from *Peeptomyces peucetius*, has been widely used to treat different cancer patients (12). ADR-induced nephrotic mouse model characterized by podocyte injury, glomerulosclerosis and tubulointerstitial inflammation (13). However, due to high accumulation in the kidney, it causes severe nephrotoxicity, such as elevated serum creatinine and proteinuria levels (13,14). In the present study, we continued to investigate STAT1-p53-p21axis involved in the development of adriamycin (ADR)-induced CN in a classical mouse model.

We present the following article in accordance with the ARRIVE reporting checklist (available at http://dx.doi.org/10.21037/atm-20-5167).

Methods

Animal preparation and establishment of ADR-induced CN model

We obtained 6-week-old male wild-type (wt) BALB/c mice (≈20 g each, n=36), from the Hebei Laboratory Animal Center (Shijiazhuang, China), and STAT1-deficient (*stat1*$^{-/-}$) mice (n=18) from Cyagen Biosciences Inc. (Guangzhou, China) Mice were housed in a pathogen-free environment under a 12-h light/dark cycle, with free access to sterilized water and a standard laboratory diet ad libitum. Temperature (24°±1°) and humidity (55%) remained constant. stat1$^{-/-}$ The ADR-induced CN model was established by a single tail vein injection of 10 mg/kg ADR (Sigma-Aldrich, St. Louis, USA) as previous described (15). Control group mice received the tail vein injection with equal volume of 0.9% saline.

Animal administration

The mice were divided into three groups: control group, wt mice treated with 0.9% saline; Model group, wt mice treated with ADR; ADR + *stat1*$^{-/-}$ group, *stat1*$^{-/-}$ mice treated with ADR. On days 14 and 28 after ADR injection, the serum and bladder urine from sacrificed mice were collected for further analysis. A portion of kidney tissues was frozen in liquid nitrogen, and the other portion was fixed in 4% paraformaldehyde. The study was approved by laboratory animal management committee of Xinxiang Central Hospital (ZXYY-KY-0039). All experiments were conducted in compliance with the National Institute of Health's Guidelines for the Care and Use of Laboratory Animals.

Proteinuria, urea nitrogen and creatinine determinations

Proteinuria levels were determined by enzyme-linked immunosorbent assay (ELISA) using a murine microalbuminuria ELISA kit (AlbuwellM™; Exocell Inc., Philadelphia, PA, USA). Urea nitrogen was detected with a QuantiChrom™ Urea Assay Kit (DIUR-500; BioAssay Systems, Hayward, CA, USA) according to manufacturer's instructions. Serum creatinine was detected with a (Enzymatic) Reagent Set from Pointe Scientific, Inc. (MI, USA).

Assessment of renal injury

Renal injury was assessed histologically with an optical microscope after hematoxylin and eosin (H&E) staining. Briefly, kidney tissue samples were fixed in 10% neutral-buffered formalin, embedded in paraffin, and sectioned at 4-μm thickness according to standard procedure. The sections were deparaffinized and hydrated gradually, and

Table 1 Primer sequences used for RT-qPCR of this study

Genes	Primer sequence (5'-3')	Length (bp)
STAT1	F: CACCCTTGCTTACTCTACTGC	122
	R: TTGAATGACTAAACGCCTGA	
p53	F: TAACAGTTCCTGCATGGGCGGC	261
	R: AGGACAGGCACAAACACGCACC	
p21	F: TGCCGCTGCCTCTTTGGT	108
	R: AAAGTCGAAGTTCCATCGCTCT	
β*AAGTCG*	F: CTGTGCCCATCTACGAGGGCTAT	155
	R: TTTGATGTCACGCACGATTTCC	

stained with H&E.

TUNEL assay

Terminal deoxynucleotidyl transferase-mediated dUTP-biotin nick end labeling (TUNEL) staining was performed according to the manufacturer's instructions (TUNEL Apoptosis detection kit; Upstate Biotechnology, Inc., Lake Placid, NY, USA) to detect apoptosis *in situ*. TUNEL-positive cells displayed brown staining of the nucleus of apoptotic cells. The extent of apoptosis was calculated by counting the ratio of TUNEL-positive tubular epithelial cells to total tubular epithelial cells in the same field.

Immunohistochemistry (IHC)

The expression of Caspase-3 was evaluated by IHC staining. Briefly, 4-μm sections of kidney tissue were deparaffinized, and endogenous peroxidase activity was blocked with 3% hydrogen peroxide at 37 ℃ for 10 min. Next, the sections were treated with 10% normal goat serum in Tris-buffered saline for 30 min at 37 ℃ and incubated overnight at 4 ℃ with Caspase-3 antibody of 1:1,000 dilution (CST, Boston, MA, USA). After washing three times with phosphate-buffered saline, the sections were incubated with secondary antibody for 30 min at room temperature, followed by the color reagent 3,30-diaminobenzidine.

Measurement of redox parameters

Blood samples were collected in each group. The generation of reactive oxygen species (ROS) in kidney was evaluated as previous described (16). The content of malondialdehyde (MDA), superoxide dismutase (SOD) and glutathione (GSH) were measured by commercially available assay kits (Jiancheng Bioengineering Institute, Nanjing, China), according to the manufacturer's proposals. The concentration of MDA is expressed as mmol/mg of protein, that of SOD as U/mg of protein and ng/L of protein for GSH.

Senescence-associated β-galactosidase (SA-β-gal) staining

Whole kidneys were fixed in 10% neutral-buffered formalin, paraffin-embedded, and sectioned at 4-μm thickness according to standard procedures. The sections were deparaffinized and hydrated gradually, and stained with freshly prepared SA-β-gal solution in the dark at 37 ℃ overnight. The percentage of cells that were positive for SA-β-gal activity was determined by counting the number of blue cells. Each experiment was repeated three times.

Real time-quantitative PCR (RT-qPCR)

Total RNA from the renal tissues was extracted with TRIzol® reagent (Invitrogen, Carlsbad, USA). The RNA was reversed into cDNA using a cDNA Synthesis Kit (Thermo Fisher, Waltham, USA) according to the manufacturer's proposals. qPCR amplification of target genes was conducted using a PCR Amplification Kit (Takara Bio, Japan). qPCR thermal cycling conditions as below: initial denaturation at 95 ℃ for 2 min, denaturation at 94 ℃ 30 sec, annealing at 55 ℃ for 20 sec and extension at 72 ℃ for 1 min (40 cycles). β-actin was normalized as the loading control gene. The primer sequences used for this work were listed in *Table 1*.

Western blots

Mouse kidneys from each group were collected for protein content testing. Total proteins were extracted with 2 mM phenylmethanesulfonyl fluoride in 1 mL ice-cold RIPA lysis buffer (Beyotime, Haimen, China). A BCA kit (KeyGEN, Nanjing, China) was used to determine protein concentrations. Proteins were resuspended in sodium dodecyl sulfate (SDS)-sample buffer, diluted in SDS buffer containing 2-mercaptoethanol (Sigma, St. Louis, MO, USA) and boiled for 10 min before loading on 12% SDS-PAGE gels. The samples were run under reducing conditions and transferred onto polyvinylidene fluoride (PVDF) membrane (Millipore, Bedford, MA, USA). After

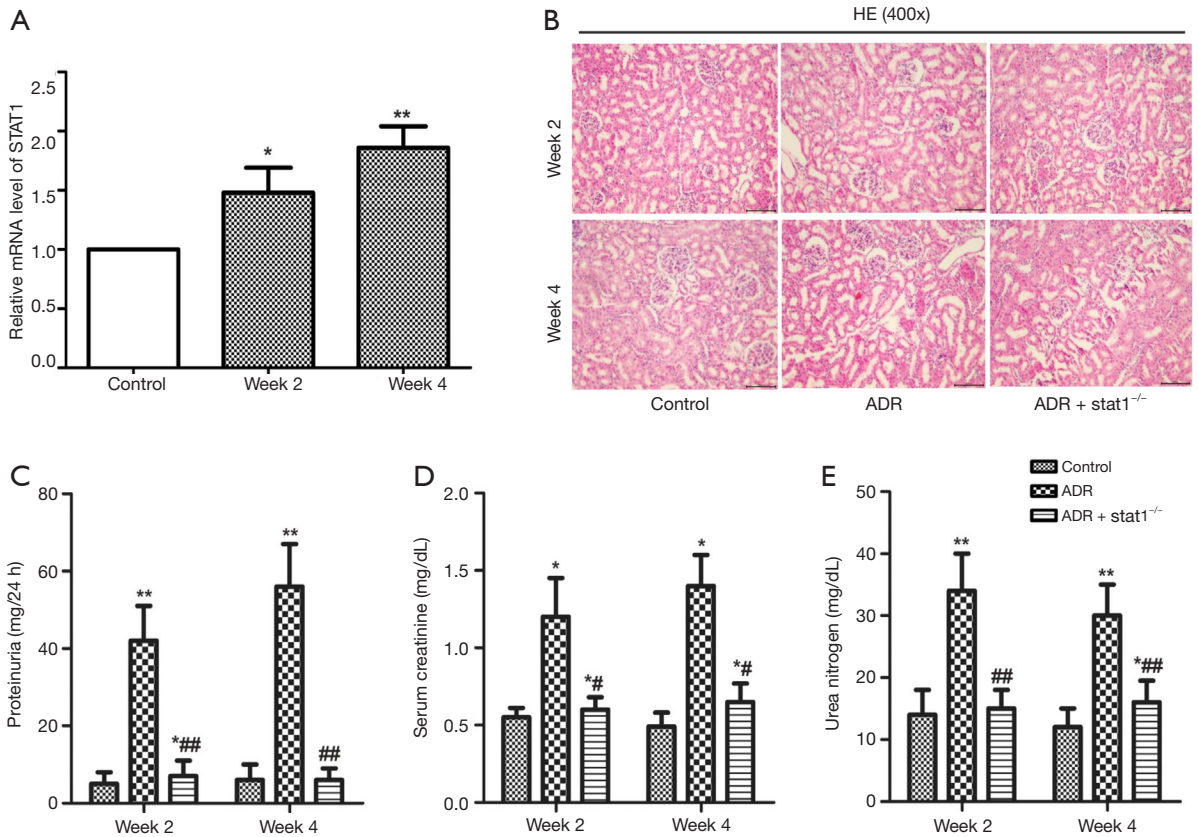

Figure 1 *stat1*$^{-/-}$ ameliorates renal injury in ADR-treated mice. (A) Relative mRNA level of expression of STAT1 was determined by RT-qPCR. (B) Representative kidney sections stained with H&E at the end of 2 weeks (upper) or 4 weeks (lower), original magnification at ×400. proteinuria, (D) serum creatinine and (E) urea nitrogen levels were detected. Data are presented as mean ± SD in three independent experiments. *, P<0.05, **, P<0.01 *vs.* control group; $^{\#}$, P<0.05, $^{\#\#}$, P<0.01 *vs.* ADR group. Scale bar =20 μm. ADR, normal wt mice treated with ADR; control, normal wt mice treated with normal saline.

blocking with 5% skim milk in Tris buffered saline Tween (TBST), the membranes were exposed to the primary antibody overnight at 4 ℃. Next day, the membranes were incubated with horseradish peroxidase (HRP)-conjugated secondary antibodies for 2 h at room temperature. The signals were visualized with enhanced chemiluminescence (Pierce, Rockford, IL, USA). β-actin was used as loading control. All antibodies from Abcam (Cambridge, UK) were listed below: Anti-STAT1 antibody (ab239360, 1:1,000); Anti-p-STAT1 antibody (ab29045, 1:1,000); Anti-p53 antibody (ab131442, 1:500); Anti-p21 antibody (ab109199, 1:1,000); Anti-Bcl-2 antibody (ab59348, 1:600), Anti-Bax antibody (ab32503, 1:600).

Statistical analysis

The data were analyzed using Graph Pad Prism version 5.0. Values are presented as mean ± SD for the indicated analyses. A probability value of P<0.05 was considered to be statistically significant for all statistical tests. Western blots were evaluated by one-way ANOVA analysis.

Results

Effects of stat1$^{-/-}$ *on morphological change in ADR-induced mice*

As shown in *Figure 1A*, qRT-PCR analysis revealed that the transcript level of *STAT1* was significantly increased in ADR mice compared with control. To address the role of *STAT1* during the development of nephrosis, we used *stat1*$^{-/-}$ mice to evaluate its effect in ADR-induced NS models, the histopathological changes of renal tubules at week 2 or 4 were observed by HE staining. As shown in

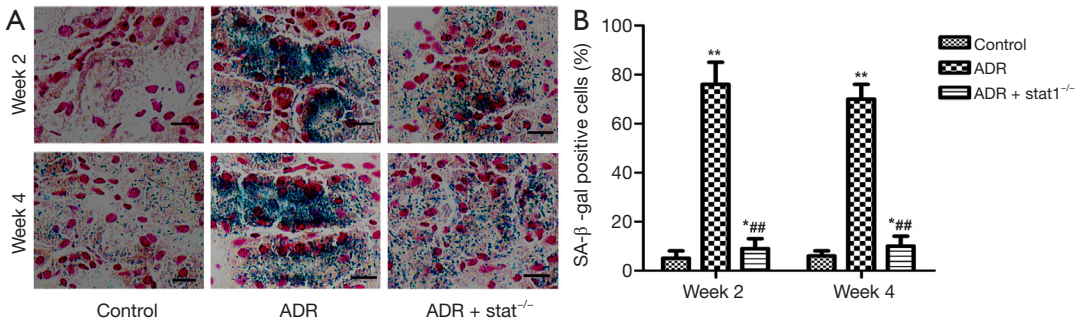

Figure 2 *stat1*$^{-/-}$ on senescence activation. (A) Senescence-associated β-galactosidase (SA-β-gal) staining of kidney tissues in the three groups (control, ADR and ADR + *stat1*$^{-/-}$). (B) Bar graph shows the percentage of SA-β-gal staining cells post 10 mg/kg ADR treatment. Data are presented as mean ± SDs in three independent experiments. *, P<0.05, **, P<0.01 *vs.* control group; ##, P<0.01 *vs.* control group. Scale bar =20 μm. GSH, glutathione; MDA, malondialdehyde; ADR, normal wt mice treated with ADR; SOD, superoxide dismutase; control, normal wt mice treated with normal saline.

Figure 1B, compared with the control group, mice treated with ADR showed epithelial cell atrophy, tubular dilatation, cellular edema and lumen cast formation accompanied by tubulointerstitial dilatation. Fortunately, the morphological changes were improved in ADR + *stat1*$^{-/-}$ group.

Effects of stat1$^{-/-}$ *on proteinuria and blood biochemistry*

As shown in *Figure 1C*,*D*,*E*, the levels of proteinuria, serum creatinine and blood urea nitrogen were elevated in ADR group compared with control group (P<0.01). The dysregulated renal function induced by ADR were significantly improved in ADR + *stat1*$^{-/-}$ group as evidenced by significant reduction of proteinuria, urea nitrogen and serum creatinine levels in ADR + *stat1*$^{-/-}$ group (P<0.01).

Effects of stat1$^{-/-}$ *on cell senescence phenotype*

STAT1 mediated senescence phenotype was determined by SA-β-gal assay. We observed that the number of these cells was higher after 10 mg/kg ADR treatment compared to control (*Figure 2A*). As shown in the bar graph, quantitative analysis showed that the percentage of SA-β-gal staining cells in ADR group was much higher than in control group (P<0.01), and the ADR + *stat1*$^{-/-}$ group exhibited fewer senescent cells, compared with ADR group (P<0.01, *Figure 2B*).

Effects of stat1$^{-/-}$ *on redox parameters*

To assess the levels of lipid peroxidation associated with ADR-induced nephrosis, ROS production and the activities of SOD, MDA and GSH in kidney tissue were determined. As shown in *Figure 3A*,*B*,*C*,*D*, ROS production and MDA content in the ADR group were much higher than in control group, whereas the activity of SOD and GSH content in the ADR group were much lower than in control group (P<0.01). Importantly, the ADR + *stat1*$^{-/-}$ group showed elevated SOD activity and GSH content and decreased ROS production and MDA compared with the ADR group (P<0.01).

Effects of stat1$^{-/-}$ *on renal apoptosis in ADR-induced mice*

The TUNEL analysis results showed that the apoptosis cells (brown) in the ADR group was much higher than in the control group (P<0.01, *Figure 4A*). In particular, the ADR + *stat1*$^{-/-}$ group attenuated cell apoptosis compared with ADR group. Furthermore, we used IHC to localize Caspase-3^{+} expression. The results revealed that the Caspase-3^{+} number of renal tissues was significantly higher than the control group, and quantitative analysis showed a significantly reduction in ADR + *stat1*$^{-/-}$ group compared with the ADR group (P<0.01, *Figure 4B*). As indicated in *Figure 4C*, the apoptosis-related proteins (Bax and Bcl-2) were investigated. We found the expression of Bax was dereased, and Bcl-2 increased in ADR + *stat1*$^{-/-}$ group, and compared with ADR group, the value of Bcl-2/Bax was increased.

Effects of stat1$^{-/-}$ *on the STAT1-p53-p21 signal axis*

We checked the mRNA and protein levels of STAT1, p53

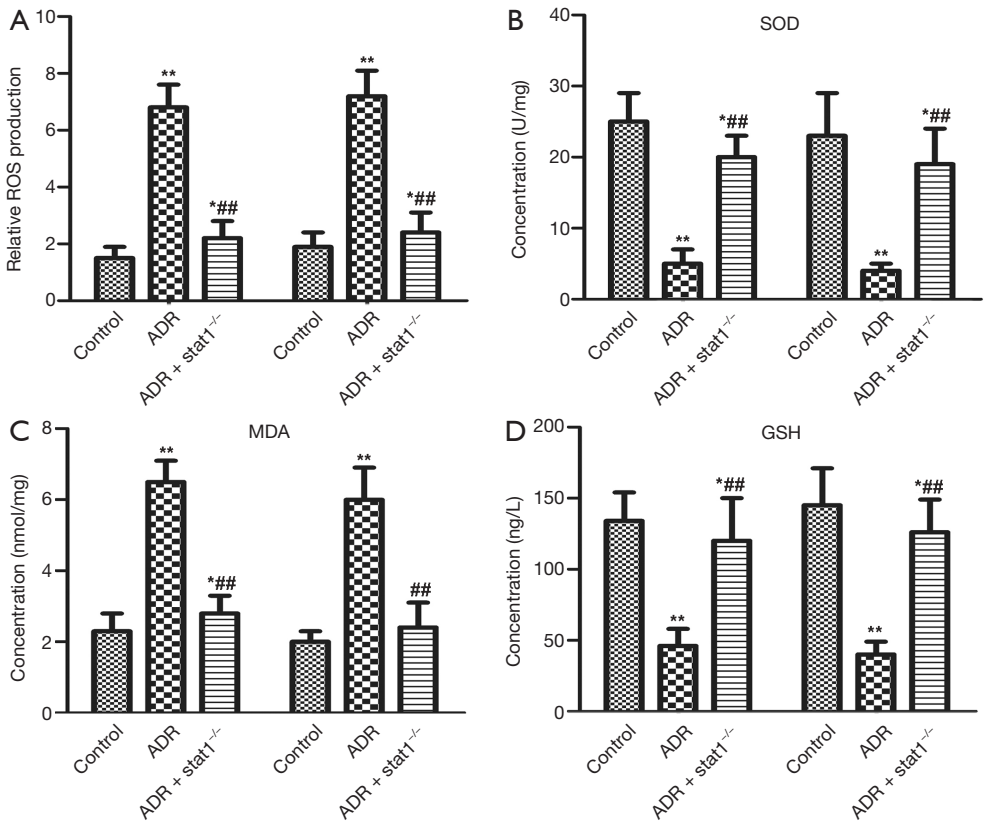

Figure 3 *stat1*$^{-/-}$ mediates oxidative stress in ADR-treated mice. Post 10 mg/kg ADR treatment, the relative (A) ROS production, (B) SOD, (C) MDA and (D) GSH concentrations were detected at the end of 2 or 4 weeks. Data are presented as mean ± SD in three independent experiments. *, P<0.05, **, P<0.01 *vs*. control group; ##, P<0.01 *vs*. ADR group. ADR, normal wt mice treated with ADR; control, normal wt mice treated with normal saline.

and p21. As shown in *Figure 5*, the mRNA levels of STAT1, p53 and p21 were significantly increased in the ADR group compared with control group (P<0.01), and the ADR + *stat1*$^{-/-}$ group showed an obvious reduction compared with ADR group (P<0.01). In addition, the protein levels of phosphorylated (P)-STAT1, p53 and p21 was significantly upregulated in ADR group compared with control group (P<0.01), and the ADR + *stat1*$^{-/-}$ group showed an obvious reduction compared with ADR group (P<0.01). Note that P-STAT1was totally blocked by STAT1 KO.

Discussion

The development of CN is usually accompanied by increased oxidative stress, apoptosis and senescence, which will accelerate deterioration in renal function (17,18). Use of ADR in rats and mice has been established as a nephrosis model (19), and recent studies have used the murine ADR-induced nephrosis model to elucidate some of the molecular details of kidney damage (20,21). The mechanism of ADR-induced CN is based on inducing podocyte apoptosis and loss of podocytes from the glomerular basement membrane (GBM), leading to glomerulosclerosis (21). In present study, we identified the systemic protective effects of *stat1*$^{-/-}$ on ADR induced CN mice. The ADR tail vein injection was widely used to establish a typical CN mouse model, which has the similar phenotype with clinical characteristics (13,14). Post modeling, (I) *STAT1* expression was increased in ADR-treated mice and very weak in *stat1*$^{-/-}$ mice; (II) *stat1*$^{-/-}$ ameliorated renal function and improved the renal tubular injury; (III) *stat1*$^{-/-}$ decreased proteinuria as well as reactive oxygen species, inhibited renal apoptosis induced by ADR.

Renal function is closely related to urine filtration, renal impairment leads to glomerular filtration dysfunction, lipoprotein deposition in glomeruli and renal tubules (22).

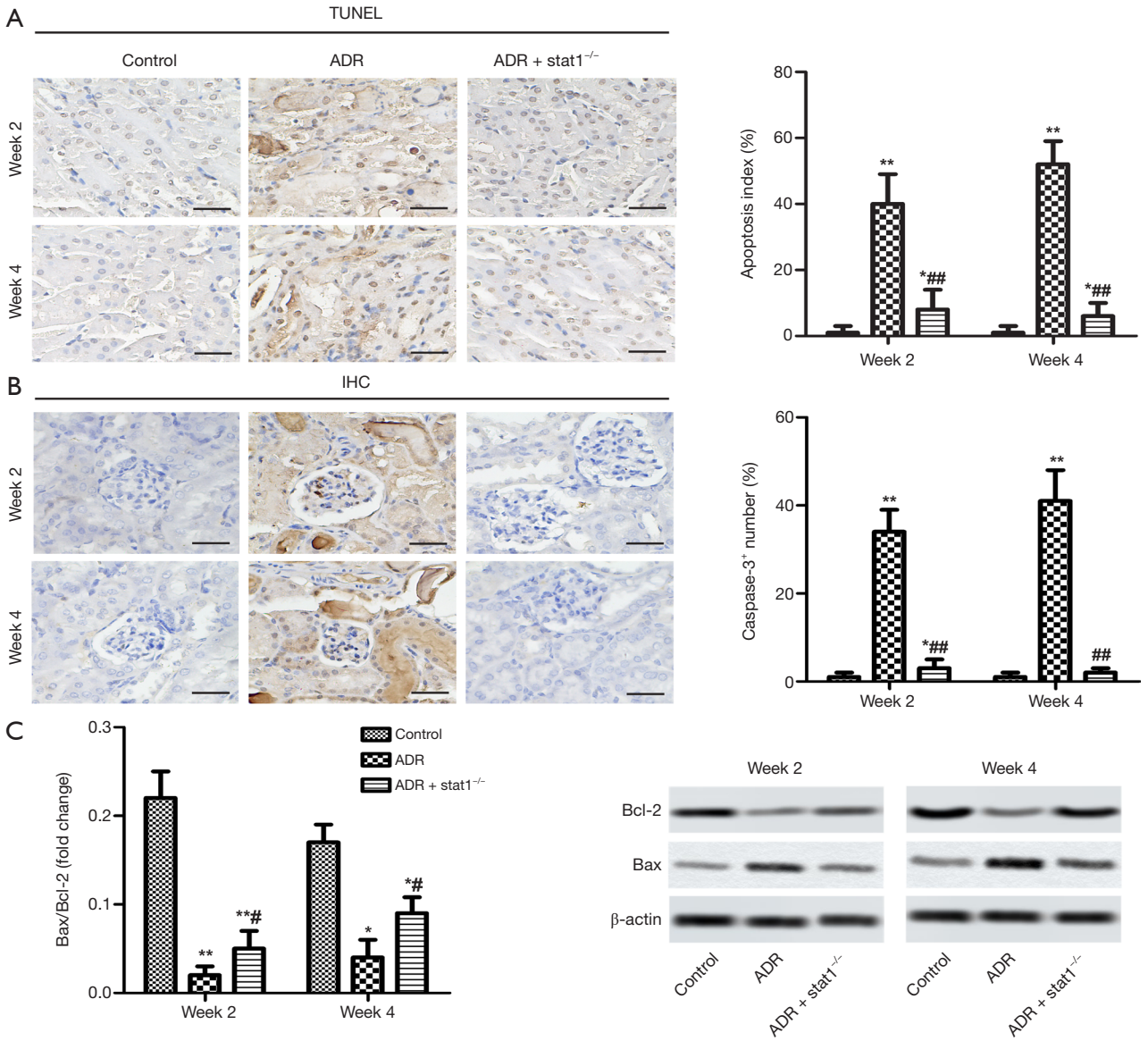

Figure 4 *stat1*$^{-/-}$ aggravates renal apoptosis in ADR-treated mice. (A) Representative photomicrographs of TUNEL staining in the kidney at the end of 2 weeks (upper) and 4 weeks (lower)in control, ADR and ADR + *stat1*$^{-/-}$ groups (original magnification at ×400), brown-staining cells were quantified as the apoptosis index. (B) Immunohistochemistry for expression of Caspase-3+ cells. (C) Relative level of protein expressions of Bcl-2 and Bax were determined by western blot. Data are presented as mean ± SD in three independent experiments. *, P<0.05, **, P<0.01 *vs.* control group; #, P<0.05, ##, P<0.01 *vs.* ADR group. Scale bar =20 μm. ADR, normal wt mice treated with ADR; control, normal wt mice treated with normal saline.

In our present study, renal tubular dilatation, epithelial cell atrophy and lumen interstitial dilatation occurred in ADR group, indicating that ADR proteinuria and hyperlipidemia caused tubular injury. However, in the ADR + *stat1*$^{-/-}$ group, proteinuria, urea nitrogen and serum creatinine decreased, the above renal tubular injury was significantly alleviated. It's reported that oxidative stress such as H_2O_2 activates STAT1 (23). STAT1 inhibition and ROS inhibition were involved in gentamicin-induced hair cell death in the Organ of Corti (24). Moreover, inactivation of STAT1 was identified as attenuating brain contusion-induced oxidative insult in rats (25). Our results showed that *stat1*$^{-/-}$ decreased

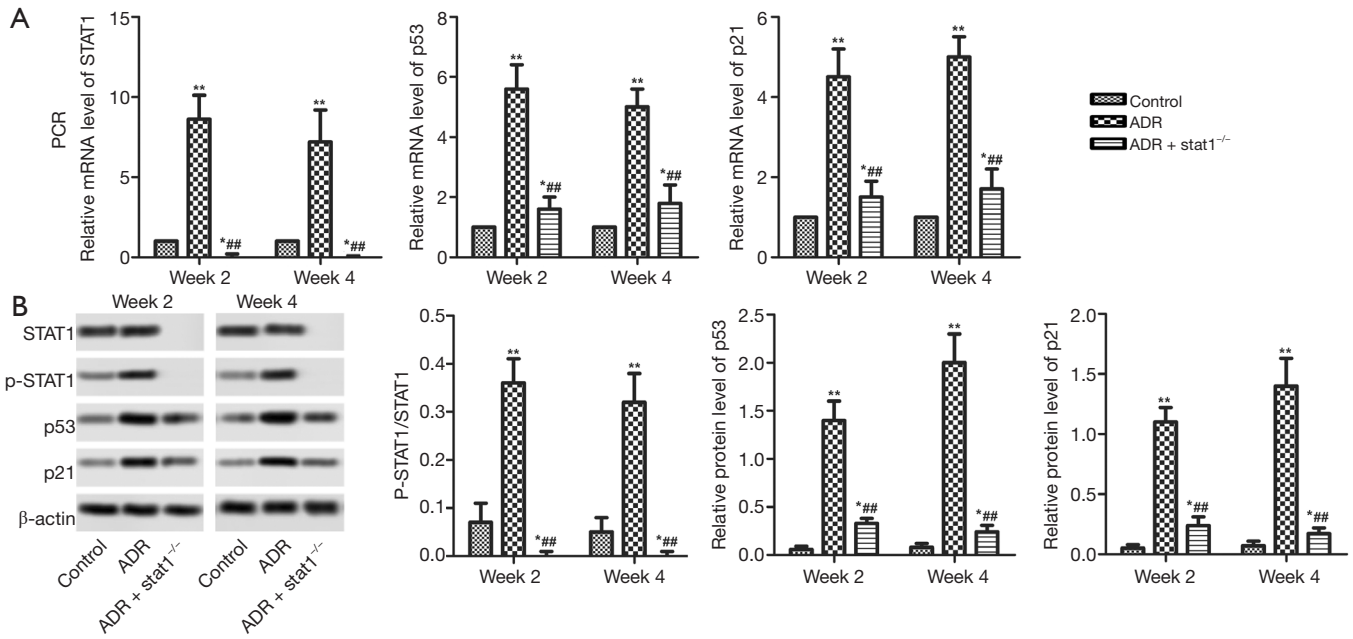

Figure 5 *stat1*$^{-/-}$ regulates the STAT1/p53/p21 axis. (A) Relative mRNA level of expression of STAT1, p53, and p21 were determined by RT-qPCR. β-actin was used as an internal control. Data are presented as the mean ± SD in three independent experiments. (B) Relative level of protein expressions of STAT1, p53, and p21 were determined by western blot. β-actin was used as loading control. Data are presented as mean ± SD in three independent experiments. *, P<0.05, **, P<0.01 *vs.* control group; ##, P<0.01 *vs.* ADR group. ADR, normal wt mice treated with adriamycin; control, normal wt mice treated with normal saline.

the ROS and MDA levels, while increasing SOD activity and GSH content. These results indicated that *stat1*$^{-/-}$ reduced oxidative stress in the ADR-induced CN mouse model. In the case of renal injury, apoptotic cell death in glomeruli or renal tubules) can lead to irreversible damage of resident cells, followed by renal disease formation (26). Caspase-dependent apoptosis signaling exerts an important role in ADR-induced apoptotic injury (27). STAT1 is reported to promote apoptosis of retinal pericytes under high glucose conditions via increasing Bcl-2-like protein 11 (Bim) expression (28). In addition, another study showed that interferon-α increased apoptosis of human hippocampal cells by activating STAT1 (29). Also, it's revealed that STAT1 downregulate Bcl-2 expression and to be involved in interferon-γ/tumor necrosis factor-α-induced apoptosis in NIT-1 cells (30). Those results suggested a positive correlation between STAT1 and apoptosis. In the present study, we demonstrated a significant increase in the percentage of apoptotic cells in kidney tissue of ADR treated mice, but *stat1*$^{-/-}$ significantly improved renal cell survival. We further examined Caspase-3 activity and key protease in ADR-induced mouse kidney tissues. The data showed that *stat1*$^{-/-}$ inhibited Caspase-3 activity and increased Bcl-2/Bax ratio, which indicated that STAT1 might have a therapeutic effect on CN by inhibiting renal apoptosis. As elaborated in our previous studies of the relationship between STAT1 and senescence (31), *stat1*$^{-/-}$ significantly inhibited the progression of HMC senescence and decreased the elevated expression of p53 and p21. Our *in vivo* study also identified the senescence suppression role of *stat1*$^{-/-}$, as shown by SA-β-Gal staining of blue cells in ADR + *stat1*$^{-/-}$ group. According to an existing study of senescence, the process has two forms: one is replication senescence, which was described by Hayflick (32) for the first time in human fibroblasts. That *in vitro* study showed cultured fibroblasts cells exhibiting permanent irreversible growth stagnation due to irreversible cell cycle arrest in the G0/G1 phase (32). The other form is stress-induced senescence, which infers that normal cells under all types of stress, such as DNA damage, oxidative stress, oncogene activation (33), etc., can quickly enter senescence and cell cycle arrest, and show some of the same characteristics of senescence as shown by the human fibroblasts, such as morphologic change, increased heterogeneity, senescence

associated β –galactosidase (SA-β-Gal) expression and fat brown pigment deposition (34). Various stimuli focus on two pathways that induce cell senescence: the p53-p21-Rb pathway and the p16-Rb pathway (35). In our study, *stat1*$^{-/-}$ totally inhibited P-STAT1 and downregulated p53 and p21, which further indicated the role of the STAT1-p53-p21 axis in the regulation of apoptosis, oxidative stress and senescence in the ADR-induced CN mouse model.

In conclusion, *stat1*$^{-/-}$ decreased apoptosis, oxidative stress and senescence in the ADR-induced CN mouse model via the STAT1-p53-p21 axis. In particular, the axis may be a potential target for CN therapy.

Acknowledgments

Funding: None.

Footnote

Reporting Checklist: The authors have completed the ARRIVE reporting checklist. Available at http://dx.doi.org/10.21037/atm-20-5167

Data Sharing Statement: Available at http://dx.doi.org/10.21037/atm-20-5167

Conflicts of Interest: All authors have completed the ICMJE uniform disclosure form (available at http://dx.doi.org/10.21037/atm-20-5167). The authors have no conflicts of interest to declare.

Ethical Statement: The authors are accountable for all aspects of the work in ensuring that questions related to the accuracy or integrity of any part of the work are appropriately investigated and resolved. The study was approved by laboratory animal management committee of Xinxiang Central Hospital (ZXYY-KY-0039). All experiments were conducted in compliance with the National Institute of Health's Guidelines for the Care and Use of Laboratory Animals.

References

1. Gambaro G, Croppi E, Bushinsky D, et al. The Risk of Chronic Kidney Disease Associated with Urolithiasis and its Urological Treatments: A Review. J Urol 2017;198:268-73.
2. Ploth DW, Mbwambo JK, Fonner VA, et al. Prevalence of CKD, Diabetes, and Hypertension in Rural Tanzania. Kidney Int Rep 2018;3:905-15.
3. Lu R, Zhou J, Liu B. Paeoniflorin ameliorates Adriamycin-induced nephrotic syndrome through the PPARgamma/ANGPTL4 pathway in vivo and vitro. Biomed Pharmacother 2017;96:137-47.
4. Locatelli F, Del Vecchio L. Are we approaching a new era in the treatment of anemia of chronic kidney disease patients? Ann Transl Med 2019;7:S333.
5. Abroun S, Saki N, Ahmadvand M, et al. STATs: An Old Story, Yet Mesmerizing. Cell J 2015;17:395-411.
6. Tao Y, Wu X, Li D, et al. Experimental study in renal protective effect of tranilast on rats with adriamycin nephropathy. Sichuan Da Xue Xue Bao Yi Xue Ban 2008;39:76-9.
7. Townsend PA, Scarabelli TM, Davidson SM, et al. STAT-1 interacts with p53 to enhance DNA damage-induced apoptosis. J Biol Chem 2004;279:5811-20.
8. Youlyouz-Marfak I, Gachard N, Le Clorennec C, et al. Identification of a novel p53-dependent activation pathway of STAT1 by antitumour genotoxic agents. Cell Death Differ 2008;15:376-85.
9. Huang YQ, Li JJ, Karpatkin S. Thrombin inhibits tumor cell growth in association with up-regulation of p21 (waf/cip1) and caspases via a p53-independent, STAT-1-dependent pathway. J Biol Chem 2000;275:6462-8.
10. Agrawal S, Agarwal ML, Chatterjee-Kishore M, et al. Stat1-dependent, p53-independent expression of p21(waf1) modulates oxysterol-induced apoptosis. Mol Cell Biol 2002;22:1981-92.
11. Fan XM, Wang ZL. Regulative Effect of STAT1 on inflammation of lung tissue in bleomycin-induced rat interstitial pulmonary fibrosis. Sichuan Da Xue Xue Bao Yi Xue Ban 2004;35:343-6.
12. Nogueira A, Pires MJ, Oliveira PA. Pathophysiological mechanisms of renal fibrosis: a review of animal models and therapeutic strategies. In Vivo 2017;31:1-22.

13. Lee VW, Harris DC. Adriamycin nephropathy: a model of focal segmental glomerulosclerosis. Nephrology 2011;16:30-8.
14. Zhang H, Ren R, Du J, et al. AF1q Contributes to Adriamycin-Induced Podocyte Injury by Activating Wnt/β-Catenin Signaling. Kidney Blood Press Res 2017;42:794-803.
15. Dong J, Jiang Z, Ma G. Hsp90 inhibition aggravates adriamycin-induced podocyte injury through intrinsic apoptosis pathway. Exp Cell Res 2020;390:111928.
16. Shan Q, Zheng GH, Han XR, et al. Troxerutin protects kidney tissue against BDE-47-induced inflammatory damage through CXCR4-TXNIP/NLRP3 signaling. Oxid Med Cell Longev 2018;2018:9865495.
17. Ali BH, Al-Salam S, Al Suleimani Y, et al. Curcumin ameliorates kidney function and oxidative stress in experimental chronic kidney disease. Basic Clin Pharmacol Toxicol 2018;122:65-73.
18. Hyde GD, Taylor RF, Ashton N, et al. Axl tyrosine kinase protects against tubulo-interstitial apoptosis and progression of renal failure in a murine model of chronic kidney disease and hyperphosphataemia. PLoS One 2014;9:e102096.
19. Bertani T, Poggi A, Pozzoni R, et al. Adriamycin-induced nephrotic syndrome in rats: sequence of pathologic events. Lab Invest 1982;46:16-23.
20. Lee VW, Harris DC. Adriamycin nephropathy: a model of focal segmental glomerulosclerosis. Nephrology 2011;16:30-8.
21. Andres-Hernando A, Li NX, Cicerchi C, et al. Protective role of fructokinase blockade in the pathogenesis of acute kidney injury in mice. Nat Commun 2017;8:14181.
22. Jiang P, Ray A, Rybak LP, et al. Role of STAT1 and oxidative stress in gentamicin-induced hair cell death in organ of corti. Otol Neurotol 2016;37:1449-56.
23. Tsai MC, Chen WJ, Tsai MS, et al. Melatonin attenuates brain contusion-induced oxidative insult, inactivation of signal transducers and activators of transcription 1, and upregulation of suppressor of cytokine signaling-3 in rats. J Pineal Res 2011;51:233-45.
24. Jiao S, Zheng X, Yang X, et al. Losartan inhibits STAT1 activation and protects human glomerular mesangial cells from angiotensin II induced premature senescence. Can J Physiol Pharmacol 2012;90:89-98.
25. Asanuma K, Akiba-Takagi M, Kodama F, et al. Dendrin location in podocytes is associated with disease progression in animal and human glomerulopathy. Am J Nephrol 2011;33:537-49.
26. Priante G, Gianesello L, Ceol M, et al. Cell death in the kidney. Int J Mol Sci 2019;20:1-21.
27. Dhuriya YK, Sharma D, Naik AA. Cellular demolition: proteins as molecular players of programmed cell death. Int J Biol Macromol 2019;138:492-503.
28. Shin ES, Huang Q, Gurel Z, et al. STAT1-mediated Bim expression promotes the apoptosis of retinal pericytes under high glucose conditions. Cell Death Dis 2014;5:e986.
29. Borsini A, Cattaneo A, Malpighi C, et al. Interferon-alpha reduces human hippocampal neurogenesis and increases apoptosis via activation of distinct STAT1-dependent mechanisms. Int J Neuropsychopharmacol 2018;21:187-200.
30. Cao ZH, Zheng QY, Li GQ, et al. STAT1-mediated down-regulation of Bcl-2 expression is involved in IFN-gamma/TNF-alpha-induced apoptosis in NIT-1 cells. PLoS One 2015;10:e0120921.
31. Burova EB, Gonchar IV, Nikol'skii NN. STAT1 and STAT3 activation by oxidative stress in A431 cells involves Src-dependent EGF receptor transactivation. Tsitologiia 2003;45:466-77.
32. Hayflick L. Entropy explains aging, genetic determinism explains longevity, and undefined terminology explains misunderstanding both. PLoS Genet 2007;3:e220.
33. Committee on the Long-Run Macroeconomic Effects of the Aging USP-P II, Committee on P, Division of B, et al. The Growing Gap in Life Expectancy by Income: Implications for Federal Programs and Policy Responses. Washington (DC): National Academies Press (US) 2015.
34. Ben-Porath I, Weinberg RA. When cells get stressed: an integrative view of cellular senescence. J Clin Invest 2004;113:8-13.
35. Muller M. Cellular senescence: molecular mechanisms, in vivo significance, and redox considerations. Antioxid Redox Signal 2009;11:59-98.

(English Language Editor: K. Brown)

Cite this article as: Wei H, Wang J, Liang Z. STAT1-p53-p21axis-dependent stress-induced progression of chronic nephrosis in adriamycin-induced mouse model. Ann Transl Med 2020;8(16):1002. doi: 10.21037/atm-20-5167

